npj | computational materials

Article

Published in partnership with the Shanghai Institute of Ceramics of the Chinese Academy of Sciences

https://doi.org/10.1038/s41524-026-01975-5

Probing multi-dimensional composition spaces in search of strong metallic alloys

Xinran Zhou[1,2,3] ✉, Jaime Marian[2], Fei Zhou[1] & Vasily V. Bulatov[1]

Refractory complex concentrated alloys (RCCA) offer exceptionally high-temperature strength compared to pure metals and dilute alloys, but predictive theory for RCCA design is lacking. We present large-scale molecular Dynamics (MD) simulations of crystal plasticity to explore alloy compositions for maximum mechanical strength, focusing on Fe-Ta-W and Nb-Ta-Mo-W alloy families modeled with Embedded Atom Model (EAM) and Spectral Neighbor Analysis Potentials (SNAP). To efficiently guide the search for strong alloy compositions, we employ iterative optimization using Gaussian process regression. Many simulated RCCA compositions exhibit pronounced cocktail strengthening, with strengths surpassing their strongest constituent metal, tungsten. Contrary to expectations, the highest strength is found on binary edges of the RCCA composition space. Detailed analyses of atomistic simulations reveal that, similar to pure BCC metals, plastic response in RCCA is primarily governed by screw dislocations. However, at large strains, dislocation multiplication and interactions (Taylor hardening) become the dominant mechanisms contributing to RCCA strength.

Developed relatively recently, the concept of complex concentrated alloys (CCA) has opened a floodgate of new research in physical metallurgy as a science of making new structural materials[1–3]. Unlike traditional materials used for millennia, CCAs are composed of several (typically four or more) elements mixed in nearly equal fractions. Opening this combinatorial 'box' of alloy compositions brings about virtually unbounded possibilities in terms of alloy chemistries and properties, making the exploration of this novel type of material both exciting and daunting. However, despite an explosive growth in CCA research and owing to difficulties in alloy synthesis and characterization, CCA developers have only explored relatively few truly distinct alloy chemistries. At the current rate of *Edisonian* exploration, much of the vast space of possible alloy compositions will remain unexplored for a long time, delaying our understanding of crucial features that govern CCA design optimization and control their properties. Theoretical models of CCAs, if sufficiently accurate and discriminating, can furnish valuable guidance to alloy developers by pointing to alloy chemistries and compositions that may be *worth trying to synthesize*.

When it comes to the mechanical strength of CCA, models have emerged in the literature building on and extending early statistical models of alloy strengthening originally developed for dilute alloys[4,5]. Just as in dilute alloys, CCA strength is ultimately defined by the interaction of dislocations with chemical disorder. However, all theoretical models of alloy strengthening so far have only considered the motion of a single dislocation immersed in a sea of alloying impurities. Yet crystal plasticity and mechanical strength are not reducible to the behavior of individual dislocations, resulting instead from complex collective interactions between large ensembles of dislocations and other crystal defects. Interactions that, in and of themselves, remain poorly understood. Performed at the limits of super-computing, here we use large-scale Molecular Dynamics (MD) simulations of model complex alloys to directly assess the effects of alloy chemistry and composition on alloy plastic strength. Rather than relying on any theoretical model, our simulations faithfully capture the full complexity of dislocation motion and dislocation interactions in complex chemical environments, and can thus be regarded as unbiased computational experiments to be used to test existing models of CCA strength and as a proving ground for further theory development. In retaining every detail of atomic motion, our MD simulations simultaneously serve as a full-resolution in silico microscope, allowing unambiguous attribution of alloy strengthening to underlying atomistic mechanisms.

Results

In this work, we focus on single-phase body-centered cubic (BCC) refractory CCA (RCCA), intensely studied by alloy developers for their demonstrated high mechanical strength retained up to high temperatures[1,6–12]. In view of the extremely high computational cost of MD simulations of crystal plasticity[13–15], here we use two computationally expedient sets of interatomic potentials available for RCCA simulations: the Embedded Atom Model (EAM) potentials[16] and the Spectral Neighbor Analysis Potentials (SNAP)[17]. We perform MD simulations of single crystals in which atoms are initially randomly placed on BCC lattice sites according to element number fractions

[1]Lawrence Livermore National Laboratory, Livermore, CA, USA. [2]University of California, Los Angeles, CA, USA. [3]Lawrence Berkeley National Laboratory, Berkeley, CA, USA. ✉e-mail: xinranz1216104@g.ucla.edu

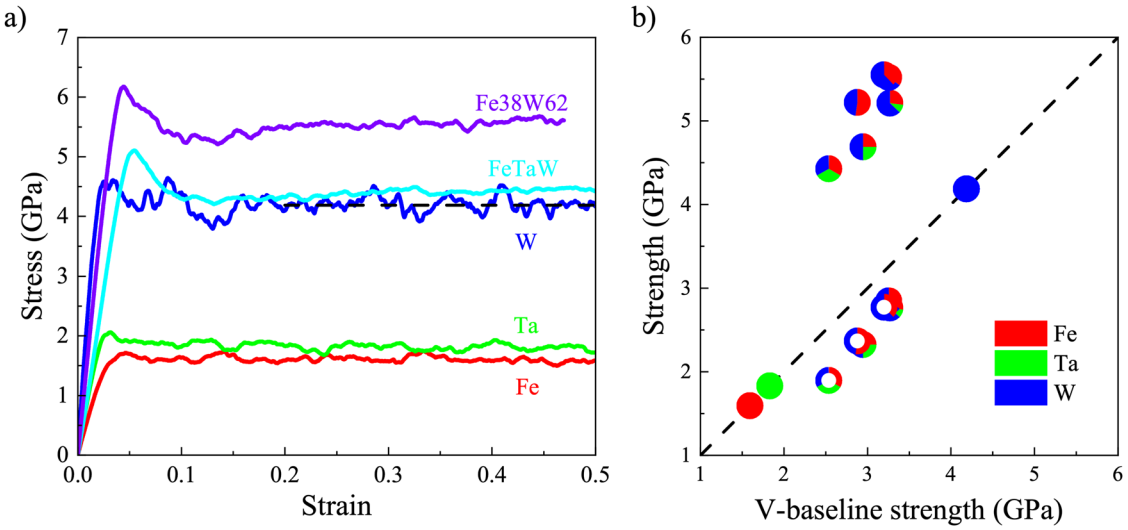

Fig. 1 | Cocktail strengthening of ternary Fe-Ta-W RCCAs predicted in MD simulations. a Full stress-strain response was observed in several molecular dynamics (MD) simulations. Metal and alloy symbols are shown next to corresponding stress-strain curves. The dashed line marks the strain interval used for flow stress averaging. **b** Full pies above the dashed line are plastic strength values predicted in MD simulations of pure metals and random solution refractory complex concentrated alloys (RCCAs), and hollow pies below the dashed line are strength values of corresponding A-atom models, both plotted against the V-baseline for strength of the same metals and alloy compositions. Colors in the pies indicate fractions of each component metal. Strength values predicted for three pure metals lie on the dashed diagonal line marking zero strengthening with respect to the baseline.

in the CCA (ideal random solid solution). Whereas atomistic simulations of CCA performed so far have only considered perfect dislocation-free crystals or at most a single dislocation in a crystal, our crystals are large enough (~33 × 10^6 atoms) to accommodate multiple dislocation sources, thus enabling all-important dislocation multiplication and dislocation collisions to proceed naturally in response to compressive straining. As a measure of mechanical strength, here we opt for the flow stress attained in steady flow regimes reached at large compressive strains ~0.5, well past few percent of strain at which the same crystals yield (Fig. 1a). Unlike the yield stress that depends on the initial dislocation microstructure, the saturated flow stress is a material property previously shown to be independent of the initial conditions in the MD simulations[14] (see also Supplementary Fig. 6). Limited by finite –albeit large– computational resources, we perform all our simulations under a true deformation rate of 10^8 s^{-1} in an *NPT* ensemble at ambient pressure and at temperature of 1000 K, i.e., in the mid-range of the temperature interval in which RCCAs are expected to retain high plastic strength (see Methods for details). Although nominally high-rate, our MD simulations are essentially quasi-static in the sense that their overall timescale of ~10 ns comfortably exceeds characteristic timescales of dynamic processes of dislocation motion and interactions as observed in the same simulations[14,15,18–20]. Furthermore, both experiments[21] and our ongoing MD simulations suggest that alloy *strengthening* (to be precisely defined below) is relatively insensitive to deformation rates.

On the short time scale of our simulations, no species diffusion is observed, thus precluding diffusional phase transformations that some of our model RCCAs would have otherwise experienced if given more time to evolve. We verified that model alloys of all compositions reported here retained single-phase BCC structures throughout MD simulations. On the upside, our MD simulations can bring out the effects of alloy composition on strength more clearly by exploring a wider range of compositions in which some of our model alloys are only metastable in the BCC phase. Consequently, our predictions should be viewed not as recommendations for practical alloy design, but rather inform alloy designers on the generic effects of chemical disorder on CCA strength.

Cocktail effect

Considering ternary Fe-Ta-W alloys modeled with EAM potentials developed in Zhou et al.[22], our first target is the elusive "cocktail" effect, whereby mixing together component metals –cocktail ingredients– may possibly result in a CCA mechanically stronger than could otherwise be expected. To quantify synergistic cocktail strengthening, it is necessary to define an expectation baseline. The simplest V-baseline is from Vegard's law [23], defined as the sum of component metal strengths weighted by each component's atomic fraction. In the following, we equate *cocktail strengthening* or simply *strengthening* to alloy strength in excess of the V-baseline strength. Another baseline previously developed specifically for EAM potentials is the simulated strength of an average atom model[24] in which all atoms are the same, but atom-atom interactions are represented by the fraction-weighted average of interatomic interactions of the component metals (see Methods). As shown in Fig. 1b and documented in Supplementary Tables 1 and 2, for all model alloys simulated with EAM potentials in this study, the two baselines are close to each other, with the V-baseline strength slightly greater than the A-baseline one for most alloy compositions. Finally, the strength of the strongest among all component metals in our model ternary alloys (tungsten) presents yet another, most stringent baseline (referred to as 'W-baseline' in the following). Regardless of which baseline is used, for consistency, all strength values should be computed under the same simulation conditions, which is precisely what we do here. As predicted by the EAM model, the Fe-Ta-W cocktails are strong with respect to all three baselines, with some compositions demonstrating extreme cocktail strengthening being markedly stronger than even the W-baseline (Fig. 1b). This observation prompted us to use the same EAM models to search for the strongest alloy composition within the Fe-Ta-W RCCA family.

GPR-guided search for strong alloy compositions

MD simulations of the kind reported here are costly, each requiring thousands of node hours on massively parallel supercomputers to complete. To reduce computational effort, we perform iterative optimization where a Gaussian process regression (GPR) surrogate model is fitted to reproduce all previously sampled strength-composition points in the Fe-Ta-W space and then used to predict the next likely composition to sample for maximum strength (see Methods for details). While never 100% exact, GPR iterations guided by MD predictions can bring the search to a composition of maximum strength. Here, we continue our iterative search until its last iteration brings no more than 3% improvement in strength, as subsequently predicted in MD. Starting from MD strengths computed for the equiatomic

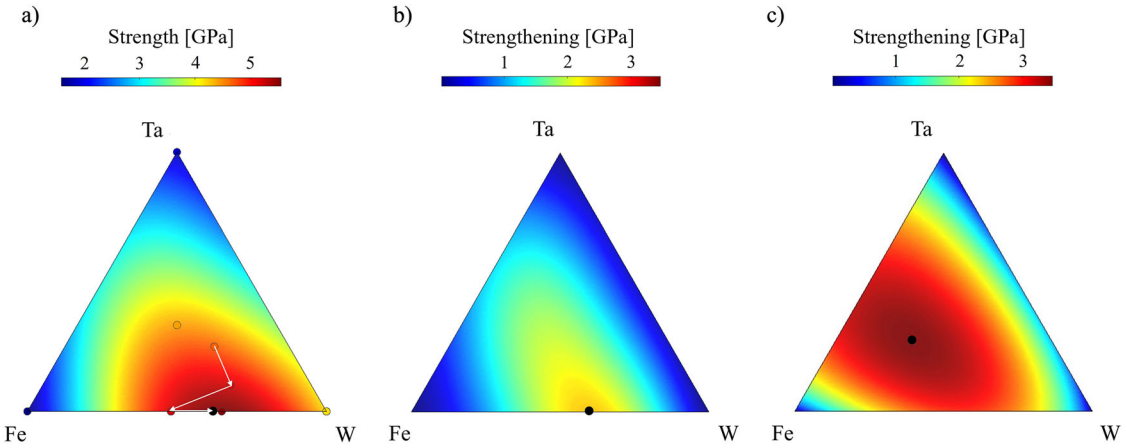

Fig. 2 | GPR-guided search for mechanically strong alloys. a The Gaussian process regression (GPR) search path in the Fe-Ta-W composition space: starting from the last of five simulated compositions selected based on intuition, four white arrows trace the sequence of four subsequent GPR predictions followed by MD simulations, eventually leading to $Fe_{38}W_{62}$ as the strongest composition. Colors over the composition triangle and the color map at the top show ranges of alloy strength predicted by a GPR surrogate model fitted to all alloy compositions for which MD simulations were performed. **b** Strengthening, defined as strength minus the V-baseline, as a function of alloy composition predicted by a GPR surrogate model fitted to nine MD simulations of Fe-Ta-W alloys. **c** Strengthening of Fe-Ta-W alloys predicted by the Maresca-Curtin edge (MCE) model. Color maps at the top of (**b**) and (**c**) show the range of predicted strengthening. Black dots mark compositions of maximum predicted strengthening.

FeTaW alloy and Fe25Ta25W50, the GPR search converged to a binary Fe38W62 composition in just four more iterations (Fig. 2a and Supplementary Table 1). For graphical representation of strength variations over alloy composition space in Fig. 2 and elsewhere, in the following, we use the standard composition triangle for ternary alloys and the composition tetrahedron (see Supplementary Information) for quaternary alloys. We performed a similar GPR-guided search for the strongest compositions among quaternary Nb-Mo-Ta-W alloys modeled with the same EAM potentials (extended by Lin et al.[25] to include Nb) as well as with the SNAP model potentials developed for the same quaternary alloy by Li et al.[26]. Detailed in Supplementary Table 2 and Supplementary Figs. 1a and 2, model EAM quaternary alloys exhibit no discernible cocktail strengthening, predicting elemental W to be the strongest system. By comparison, the same Nb-Mo-Ta-W alloys modeled with the SNAP potentials show minor cocktail strengthening over the V-baseline (A-models are not defined for SNAP potentials) and perhaps even slight strengthening over the W-baseline (Supplementary Table 3 and Supplementary Figs. 1b and 2). Minor discrepancies in predicted strengthening notwithstanding, an iterative search for the strongest alloy over the composition space of SNAP quaternaries quickly converges to a tungsten-rich alloy (Supplementary Fig. 1b). We note that despite minor difference between the SNAP and the EAM models in predicting the strongest ternary compositions, strength of the tungsten-rich composition predicted to be strongest by the SNAP model is within 2% of strength predicted by the same SNAP model for the unalloyed tungsten. Variations among predictions between two model potentials observed in this instance provide a measure of overall uncertainty in our MD predictions of strength. In parallel, we also performed GPR-guided MD simulations in search of alloy compositions of highest *specific strength* defined as the ratio of alloy strength to alloy density, an important parameter for technological applications requiring strong lightweight materials (see Supplementary Tables 1, 2 and 3 and Supplementary Figs. 4 and 5).

Comparison to the Maresca-Curtin edge model

Among theoretical models proposed so far for predicting the strength of complex BCC alloys[27–31], we opt to compare our MD simulations to the model proposed by Maresca and Curtin ('MCE' model in the following) in which alloy strengthening is assumed to result from interactions between edge dislocations and a sea of substitutional impurities[28,30]. As detailed in Methods, for direct comparison to our MD predictions, the MCE model had to be rescaled to the high deformation rates employed in our simulations and adjusted for the high strength of component metals not accounted for in the MCE model. Shown in Fig. 2b and c, variations of the strengthening over the composition space of ternary Fe-Ta-W alloys predicted by the MCE model differ both quantitatively and qualitatively from our MD predictions, even though the same EAM interatomic potentials were used in our MD simulations and in computing material parameters entering the MCE model. Compositions of predicted maximum strengthening are quite different: binary Fe38W62 from our MD simulations versus ternary Fe40Ta30W30 from the MCE model.

Deformation microstructure

Full atomistic resolution of our MD simulations permits in-depth examination of the origins of strengthening in RCCA. In particular, our MD data reveals which dislocation line orientations—screws as proposed in Rao et al.[31], or edges as in the MCE model—experience greater lattice resistance to dislocation motion. $\frac{1}{2}\langle 111\rangle$ dislocations with line orientation parallel to the Burgers vector (screws) are known to be much less mobile than dislocations of non-screw orientations in BCC metals and dilute alloys at low and intermediate temperatures. One prominent manifestation of such mobility anisotropy is numerous TEM observations of long straight screws drawn by more mobile non-screw segments of the same dislocations gliding out of existence after a moderate amount of plastic deformation[32,33]. The same anisotropy has been confirmed to persist in high-rate MD simulations of pure BCC metals[14,18]. If edge dislocations were to experience greater lattice resistance than screws—the key assumption in the MCE model – edge line orientations should become similarly over-represented over the screws in plastically deformed RCCAs. Figure 3a, b present two in silico "micrographs" extracted using the DXA algorithm in `OVITO`[34] at the end of the corresponding MD simulations. Visual inspection reveals comparably dominant presence of screws (red lines) in elemental W and in the Fe38W62 RCCA, which becomes more evident from Fig. 3c and d showing detailed distributions of dislocation line characters computed at different stages of straining. Clearly, screw dislocations become just as over-represented in RCCA as in pure W. A slight redistribution of dislocation orientations from exact screws to near-screws is observed, reflecting the well-recognized waviness of screw dislocations in RCCA caused by chemical disorder[28,35].

Further evidence for an essential role of screw dislocations in RCCA plasticity is presented in Fig. 3e, f, showing defects other than dislocations generated under identical deformation conditions in pure W and a binary RCCA. Copious amounts of gray features seen in two snapshots at the very

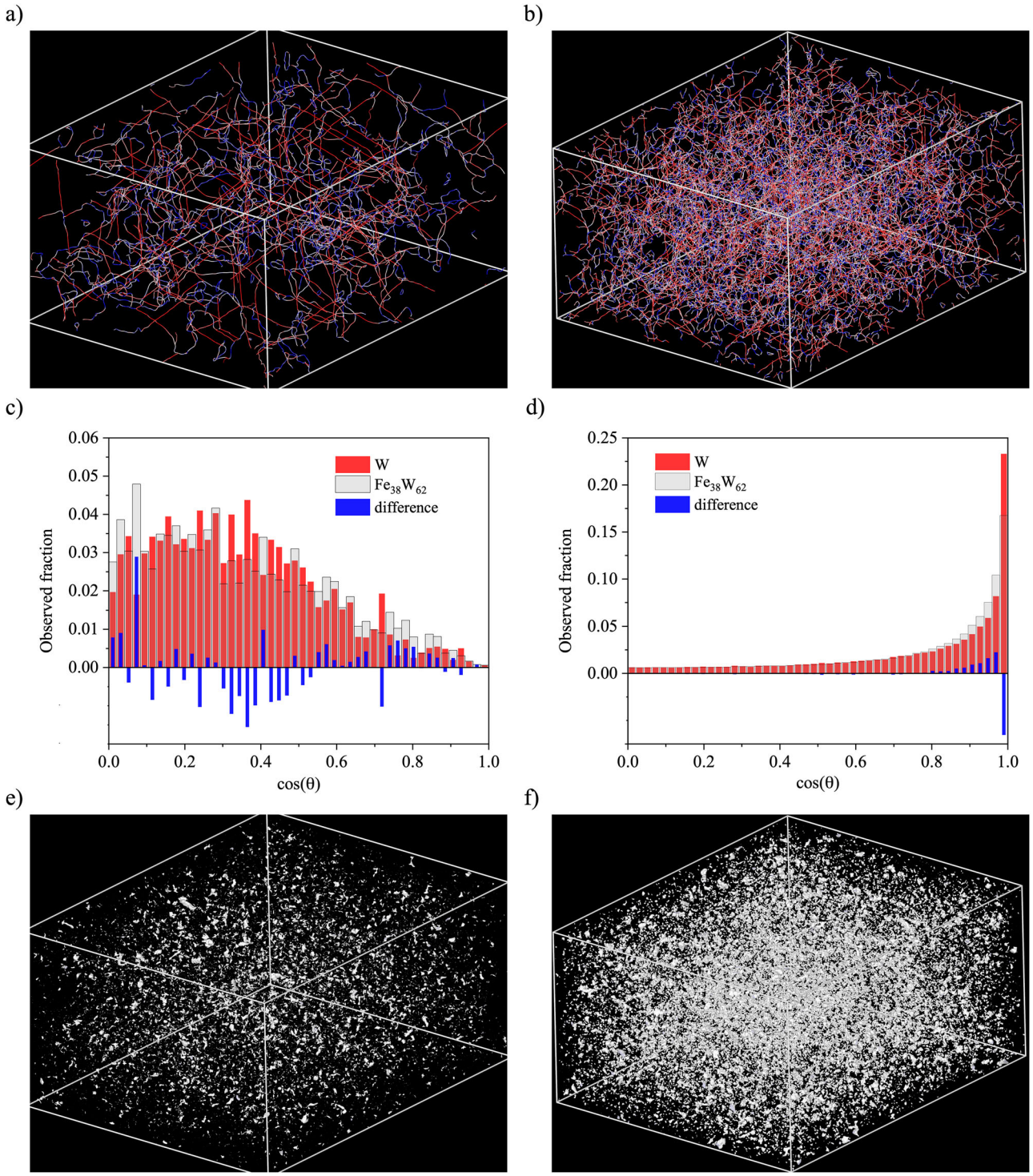

Fig. 3 | Defect microstructures attained under compressive deformation of pure W and $Fe_{38}W_{62}$ binary alloy. a Dislocation network in W and **b** in $Fe_{38}W_{62}$. Dislocation lines are colored according to their orientations with respect to their Burgers vectors: red lines indicate screw dislocations and blue lines indicate edge dislocations. **c** Distribution of dislocation characters in the beginning and **d** in the end of the same two MD simulations. The histograms are binned on the cosine of the dislocation character angle. The histogram colors indicate different dislocation types. **e** Debris defects in W and **f** in $Fe_{38}W_{62}$: gray blobs enclose atoms outside of dislocation cores deemed "not body-centered cubic (BCC)" by the adaptive common neighbor analysis (CNA) algorithm[53].

end of the simulated compression enclose vacancies, self-interstitials, and clusters thereof. The concentration of such defects is zero initially but is seen to steadily grow over the course of deformation. The origin of such defects is in self-pinning of screw dislocations as a consequence of kink-pair nucleation on two different glide planes[35,36], a mechanism significantly raising lattice resistance to dislocation motion and operating only on screw dislocations. The debris density in RCCA is about two times greater than in pure W, suggesting that self-pinning of screw dislocations offers markedly greater resistance to dislocation motion in RCCA than in W. This is consistent with earlier observations that, owing to chemical disorder, screw dislocations can form cross-kinks in RCCA even at rest under zero stress[28,37]. In addition to cross-kinks, jogs resulting from dislocation intersections add

resistance to dislocation motion and can similarly produce point defects and defect clusters.

Taken together, these results indicate that forest hardening naturally emerges as the dominant contribution to plastic strength in RCCA, in contrast to the assumption of the MCE theory, which neglects dislocation-dislocation interactions. Unlike the MC framework, which attributes strengthening to isolated edge dislocations, our molecular dynamics simulations explicitly capture collective interactions between screw and edge segments. As a result, forest hardening arises spontaneously rather than being imposed by initial conditions. The observed discrepancy between our results and the MC theory, therefore, highlights the need for theoretical models of random solid-solution alloys to incorporate dislocation interaction and multiplication effects to realistically describe alloy strengthening.

Taylor hardening

Overall, Fig. 3 makes a strong case for a dominant role of screw dislocations in the plastic response of BCC metals and RCCA alike. However, our MD simulations show that plasticity in BCC crystals cannot be reduced to the behavior of individual dislocations, screw or edge, revealing instead that dislocation-dislocation interactions contribute decisively to flow stress. Not presently accounted for in theoretical models of RCCA strength, the contribution of dislocation interactions to the flow stress is well captured by the venerable Taylor hardening equation[38]

$$\tau = \alpha \mu b \sqrt{\rho}, \tag{1}$$

where τ is the flow stress, μ is an elastic stiffness modulus, b is the Burgers vector, and α is a dimensionless hardening coefficient accounting for the holding strength of dislocation network junctions. Attributed to additional resistance to dislocation motion caused by intersecting dislocations that multiply under deformation[39], Taylor (network) hardening has been widely observed and quantified in a wide variety of crystalline materials. In pure (unalloyed) FCC metals, network hardening makes a dominant contribution to plastic strength at quasistatic ($\sim 10^{-4}/s$) laboratory tests[40–44]. This dominance persists at high rates ($\sim 10^{8}/s$) of our MD simulations, manifesting itself clearly in flow stress closely tracking the square root of dislocation density over long deformation paths in FCC aluminum (Fig. 4a and b). Taylor hardening has been similarly observed in laboratory tests of BCC metals[45,46], however, in our high-rate MD simulations of BCC metals and RCCAs, no hardening of any kind is observed past initial yield: the flow stress remains very nearly constant under continued deformation (Fig. 1a and Supplementary Fig. 4) even though dislocation density rises by a substantial factor. Apparent lack of hardening under high-rate deformation conditions was proposed[14] to result from nearly complete compensation of lattice resistance and network resistance, one falling and the other simultaneously rising as dislocations multiply under continued deformation. Well-resolved Taylor hardening in low-rate experiments and no or little hardening in our high-rate MD simulations are reconciled by observing that lattice resistance in BCC materials is highly rate-dependent and decreases rapidly—linearly (edge dislocations) or even super-linearly (screw dislocations)—with decreasing deformation rates, whereas network (Taylor) resistance closely follows the dislocation density that decreases with rates much more slowly. This is further illustrated in Fig. 4c, where Taylor hardening past yield in BCC tantalum becomes increasingly noticeable at lower deformation rates.

Given their exorbitant computational cost, we have not performed RCCA simulations at rates lower than $10^{8}/s$; however, the close similarity of plasticity response of pure BCC metals and RCCAs (see Fig. 3) suggests that our MD simulations of BCC tantalum shown in Fig. 4c are qualitatively representative of RCCAs as well. Indeed, we observe the same interplay between lattice and network resistance in RCCA, both enhanced in comparison to elemental BCC metals. Owing to chemical disorder reflected in enhanced self-pinning of screw dislocations (compare Fig. 3e and f) lattice resistance should be substantially greater in RCCA than in W, but so should be the network resistance given that dislocation density attained in the RCCA (Fig. 3b) is 3.3 times greater than in BCC W (Fig. 3a). Remarkably, having attained their corresponding states of steady plastic flow, all BCC component metals and all binary, ternary and quaternary RCCAs examined in our MD simulations fall close to a straight line with slope 1.0—the solid black line in Fig. 4d—of classical Taylor hardening (Fig. 4d). A linear best fit to the data points on the same log-log plot yields an intercept corresponding to Taylor hardening coefficient $\alpha = 0.25$ which is within the range of 0.2–0.35 quoted in the literature for parameter α in pure BCC metals and dilute alloys[47]. Remarkably simple, when the Taylor hardening equation holds, it is a sign that flow stress is defined by network resistance to dislocation motion. Its applicability was recently verified even for colloidal crystals in which shear modulus, the Burgers vector and dislocation densities differ by many orders of magnitude from those in FCC or BCC metals[48]. We posit that, despite lattice resistance to dislocation motion being high in BCC metals and further enhanced by chemical disorder in RCCAs, on reaching sufficiently large strains, network resistance becomes the dominant contribution to flow stress. We expect that, similar to elemental BCC metals, the cross-over point at which network resistance becomes dominant, and the Taylor equation begins to hold in RCCA, shifts towards lower strains with decreasing straining rates. In a state where flow stress is defined by Taylor hardening, the rate and temperature dependence of flow stress are defined by the rate and temperature dependence of dislocation multiplication and annihilation. We further conjecture that, although lattice resistance can make a large or even possibly dominant contribution to plastic strength of BCC materials at initial yield, network resistance (Taylor hardening) defines plastic strength at large strains, thus bearing on ultimate strength and ductility, i.e., the material's ability to remain strong at larger strains well past yield.

Discussion

Having established that the plastic strength of BCC materials is inextricably controlled by both lattice and network contributions, next we turn our attention to the reasons behind the higher strength of RCCA relative to elemental BCC metals. Naturally, compositional complexity comes to mind as the decisive factor enhancing RCCA strength, as it relates to both lattice and network strengthening. Prior studies point to atomic size misfit, an inevitable consequence of high chemical disorder in crystals, as the main culprit in enhanced lattice resistance in complex alloys[24,29]. When it comes to enhanced Taylor hardening, it is not clear exactly how compositional complexity magnifies dislocation multiplication relative to that in pure metals. Here, we speculate that enhanced dislocation multiplication observed in our simulations of RCCA may share its origin with the increased lattice resistance clearly observed in the same simulations. This is substantiated by observations of profuse cross-kinking on screw dislocations induced by chemical disorder in RCCA. Resulting from collisions of kinks moving on non-parallel glide planes[35,36], cross-kinks act as strong pinning points that can only be resolved by emitting point defects or defect clusters in the form of prismatic 'debris' loops. In MD simulations of sufficiently long (~1000b) individual screw dislocation lines under conditions similar to MD simulations reported here, we observe some of the larger emitted debris loops to subsequently rotate and extend into dipoles of two new screw dislocations. We estimate that stress attained in our MD simulations of RCCA should be sufficiently high for such a self-multiplication mechanism to operate.

Designed as computational experiments, our large-scale MD simulations reveal a complex interplay of plastic flow mechanisms in compositionally complex alloys, some of which remain unaccounted for in existing theoretical models of RCCA strengthening. Critical among deficiencies uncovered in our simulations is disregarding the contribution of dislocation multiplication and dislocation network resistance (Taylor hardening) to alloy strength while relating RCCA strength solely to mobility properties of individual dislocations (lattice resistance). Even if chemical disorder raises both the lattice resistance and the network resistance in RCCA, the latter becomes increasingly dominant with increasing plastic strain and/or decreasing deformation rates. To mitigate the combinatorial cost of

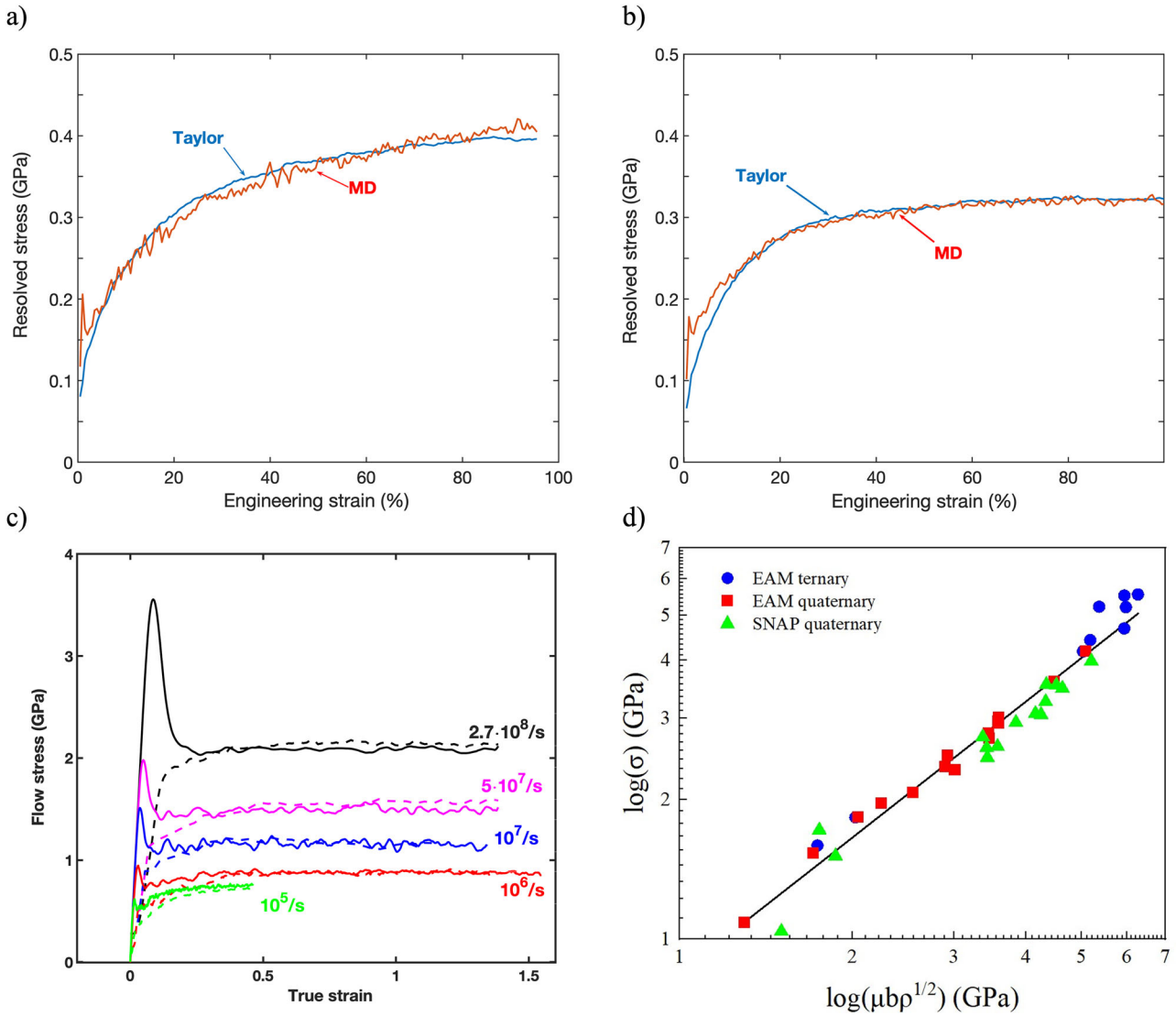

Fig. 4 | Taylor hardening in metals and alloys. a Red line is resolved flow stress as a function of strain from an MD simulation of face-centered cubic (FCC) aluminum subjected to uniaxial tensile deformation along the [001] axis at a strain rate of $5 \cdot 10^7/s$ and temperature of 300 K (previously unpublished data from ref. 15). The blue line is the same stress predicted using the Taylor equation with the parameter α equal to 0.257 and the dislocation density observed in the same simulation. **b** Same as (**a**) but for tensile deformation along the [111] axis and Taylor equation prediction with α equal to 0.21. **c** Solid lines show stress on the maximum resolved shear stress planes in BCC tantalum from MD simulations of uniaxial compression along the [100] axis at 300 K at five different deformation rates. Dashed lines show flow stress predicted for the same deformation rates using the Taylor equation with α equal to 0.32. **d** Steady flow stress on the maximum resolved shear stress planes is plotted against the square root of the dislocation density ρ from MD simulations of pure BCC metals and RCCAs under uniaxial compression along the [001] axis at a strain rate of $10^8/s$ and 1000 K. To obtain the Taylor equation prediction on the horizontal axis, $\sqrt{\rho}$ was multiplied by the Voigt average shear modulus μ and the Burgers vector b, computed separately for each model material. The Burgers vectors and the shear moduli were computed individually for every alloy composition presented on the plot in (**d**) at ambient pressure and the same temperature, 1000 K, as in all our MD simulations of alloy strength.

searching for mechanically strong alloys in RCCA composition spaces, we employ iterative optimization using Gaussian process regression. At variance with existing literature, compositions of maximum strength are found on a binary edge of the composition space (in Fe-Ta-W alloys) or at or near the strongest component metal W (in Nb-Mo-Ta-W alloys). Of the two alloy families examined here, only the ternary Fe-Ta-W alloys exhibit prominent cocktail strengthening, whereas quaternary Nb-Mo-Ta-W alloys do not which is attributed to a significantly greater size misfit between smaller Fe atoms and larger Nb, Mo, Ta and W atoms. In the absence of a significant size mismatch, compositions of maximum strength are found at larger fractions of elastically stiff component metals. Rather than practical recommendations for alloy design, at present we regard our simulations as a means to test existing theoretical models and to reveal relevant atomistic mechanisms of alloy strengthening, thus serving as a proving ground for yet to be developed quantitative theory of RCCA strength. We envision that, in synchrony with the ongoing explosive development of quantum-accurate interatomic potentials for complex materials, combining large-scale MD simulations with iterative optimization can become an efficient and increasingly accurate approach for computational *pre-design* of mechanically strong complex alloys.

In interpreting these findings, it is important to introduce a relatively high initial dislocation density to ensure that dislocation glide governs plastic deformation under quasistatic conditions. This setup is not meant to reproduce experimental microstructures but to suppress nucleation-controlled mechanisms such as twinning or displacive transformations that would otherwise dominate at high MD strain rates. Given the limited system sizes accessible to MD, a sufficient initial dislocation population is required to realize a 'dislocation-only' response. Notably, the steady-state

flow stress and dislocation density are largely independent of the initial density, although reaching the same state from a lower density would require unrealistically long simulation times.

Methods

MD simulations

All MD simulations were performed on the Lassen supercomputer at LLNL using the KOKKOS GPU implementation of LAMMPS code[49] with EAM potentials developed by Zhou et al.[22] and SNAP potentials developed by Li et al.[26]. BCC crystals comprised of about 33 million atoms and oriented along $x = [100]$, $y = [010]$, $z = [001]$ were generated with periodic boundary conditions enforced in all three dimensions. To simulate random solid solutions, atom species were randomly distributed at proportions determined by ratios of constituent components in each target alloy. Following the methodology described in detail in ref. 14 the crystals were seeded with dislocation loops at initial dislocation density $\rho_{disloc} = 2 \times 10^{15}/\mathrm{m}^2$, followed by annealing using *nph* barostat at zero pressure and *langevin* thermostat at 1000 K. Starting from an initial aspect ratio 4:2:1, uniaxial compression was applied along the x-axis of the crystal at a constant strain rate $\dot{\epsilon} = 10^8/\mathrm{s}$ under continued coupling to a *nph* barostat and a *langevin* thermostat to sustain a uniaxial stress state and the same constant temperature 1000K. All simulations were performed using a time step $dt = 10^{-2}$ ps. Dislocation and debris defects were extracted using the DXA algorithm[50], and the resulting configurations were visualized in OVITO[34].

Average atom potentials used in MD simulations of A-baseline models had the same functional form as the original EAM potential[22] with the potential energy of an atom i given by:

$$E_i = \sum_i F^A(\overline{\rho}_i) + \frac{1}{2}\sum_{i,j\neq i} \phi_{ij}^{AA}, \tag{2}$$

$$F^A(\overline{\rho}_i) = \sum_\alpha c_\alpha F^\alpha(\overline{\rho}_i), \tag{3}$$

$$\overline{\rho}_i = \sum_{j\neq i}\sum\nolimits_\alpha c_\alpha \rho_{ij}^\alpha. \tag{4}$$

$$\phi_{ij}^{AA} = \sum_{\alpha.\beta} c_\alpha c_\beta \phi_{ij}^{\alpha\beta}, \tag{5}$$

Here, F is the embedding function, $\overline{\rho_i}$ is the electron charge density at the location of atom i supplied by its neighbors j and ϕ_{ij} defines the pair-wise interaction between atoms i and j. Superscript A pertains to the average atom model, whereas α and β index chemical identities of atoms i and j.

Iterative Gaussian process regression

To guide our search for mechanically strong alloys in the space of alloy compositions, we used Gaussian process regression (GPR) models implemented in Scikit-learn[51]. GPR is a nonlinear, non-parametric regression method widely used for interpolating between data points scattered in a high-dimensional input space. In comparison with other ML algorithms for non-linear regression, GPR works particularly well on small data sets, requires no cross-validation and can be adequately trained on a limited number of inputs. Here, instead of training once for good, our GPR model evolves through a series of training iterations on a dynamically enlarging training set, aiming to improve the overall performance step-by-step. Initially, the model is trained using a small set of alloy compositions (inputs) and their corresponding strength values computed in MD simulations (labels), typically containing all elemental metals and a few symmetric alloy compositions, e.g, equiatomic. Next, the model is used to predict a composition of the highest strength, followed by an actual MD simulation of the just proposed alloy composition. After adding the newly computed composition and its plastic strength to the training set, the GPR model is retrained and used to propose yet another composition of maximum strength. By repeating such prediction-sampling-training iterations, the accuracy of model predictions gradually improves. Iterations terminate when the maximum strength predicted by the last retrained model is within 3% of the strength of the last simulated alloy composition. The latter strength is taken as the final prediction for the mechanically strongest composition within the family of alloys being investigated. To maintain a good balance between interpolation and extrapolation and to enable reasonably accurate predictions of unseen samples, for the GPR kernel, we used a combination of the linear kernel and the Radial basis function kernel and the L-BFGS-B algorithm for optimization[51].

Comparing MD simulations to predictions of the Maresca-Curtin edge model

The Maresca and Curtin edge (MCE) model assumes that CCA strengthening results from interactions between edge dislocations and a sea of substitutional impurities[28,30]. Building on the classical statistical theory of metal strengthening developed by Labusch for dilute alloys[5,52], the MCE model is perturbative in predicting not strength, but strengthening, i.e., strength added to that of a pure base metal caused by dislocation-solute interactions. While extending to concentrated alloys a perturbative theory developed for dilute alloys appears problematic, MC makes their development more palatable by defining their unperturbed host matrix material not as a base unalloyed metal, but as a hypothetical average atom material in which atom-atom interactions are averaged over interactions in pure metals with weights equal to fractions of each constituent element. Noting that an infinite number of possible ways can be devised to average over atom-atom interactions, none of them correct a priori, local chemical perturbations are indeed minimized with respect to the so-defined composition-dependent reference material. MC opted to use a convenient mixing rule for defining cross-interaction potentials proposed by the original developers of the EAM potentials used here[22] and defined in Eqns. 3-6.

We observe that the already mentioned distinction between strength and strengthening is often ignored in the literature altogether[28,30] which can be justified for FCC materials since the strength of pure FCC metals under low deformation rates is indeed very low (~ 1 MPa) and can be neglected by comparison to a much greater strength of dilute and even greater strength of concentrated FCC alloys. However strength of pure BCC metals can be quite high even under low deformation rates (nearly 1 GPa for W) and becomes still higher with increasing straining rates. Not subtracting a baseline strength from our MD simulation predictions for alloy strength would have resulted in gross discrepancies between MD predictions and the MCE model. In particular, as a perturbative model and as it should, the MCE model predicts zero strengthening for alloy compositions corresponding to pure metals, whereas the strength of pure metals predicted in our MD simulations constitutes a large fraction of the total strength, even for the strongest simulated alloy cocktails. Therefore, for consistency, in Fig. 2b, c we compare our MD simulations to MCE model predictions only after subtracting from each value of strength predicted in MD the strength computed for the same alloy composition from its A-baseline model.

As discussed in ref. 29, the MCE model is nominally defined for deformation rates below 10^4/s; however, scaling of yield strength between high to low deformation rates is performed in an ad hoc manner common in the literature, yet inconsistent with physical observations. In using Orowan's kinematic relation to connect macroscopic yield stress to mobility of non-interacting dislocations—an assumption of "ideal gas of dislocations" common to most, if not all, existing models of alloy strengthening—the MCE model neglects any possible effects of dislocation multiplication and dislocation interactions. Furthermore, the term defining scaling of yield strength with deformation rate in the MCE model implicitly assumes that dislocation density at yield remains the same over the entire range of deformation rates below 10^4/s, thus completely ignoring the rate dependence of dislocation multiplication. Yet, over the range of rates where the MCE model is assumed to be applicable dislocation density attained in a plastically deformed crystal varies by several orders of magnitude. Such variations can not be discounted even if dislocation density enters the equation for yield stress under a logarithm as it does in the MCE model. To

enable comparisons to our high-rate MD simulation results, we modify the MCE model equation for yield stress by inserting in it dislocation density ρ observed in our MD simulations resulting in the following adjusted form of MCE model

$$\tau_y = \tau_{y0} \cdot \left\{ 1 - \left[\frac{k_B T}{E_b} \log\left(\frac{\rho b v_0}{\dot{\varepsilon}} \right) \right]^{2/3} \right\} \quad (6)$$

where τ_{y0} and E_b are a zero-temperature glide stress and an activation energy barrier, k_B is the Boltzmann constant, T is temperature, ρ is composition-dependent dislocation density, b is the Burgers vector and v_0 has the meaning of marginal dislocation velocity above which dislocation motion no longer proceeds via kink pair nucleation mechanisms. Here we set v_0 = 100m/s. To be able to compute MC model predictions using equation (6), it is necessary to account for substantial variations of dislocation density over the space of alloy compositions. For this purpose, we fitted a GPR surrogate model to dislocation density values attained in our MD simulations of actually sampled alloy compositions. To obtain τ_{y0} and E_b, which both depend on atomic size misfit and elastic constants as described in ref. 29, we additionally calculated lattice parameters and elastic constants for SNAP and EAM interatomic potential models at 1000K and ambient pressure.

Data availability

All data required to reproduce findings presented in this paper can be shared upon reasonable request to the corresponding author of the paper.

Code availability

LAMMPS software used in all MD simulations reported in this work is available at https://www.lammps.org.

Received: 9 May 2025; Accepted: 15 January 2026;
Published online: 31 January 2026

References

1. Senkov, O. N., Miracle, D. B., Chaput, K. J. & Couzinie, J.-P. Development and exploration of refractory high entropy alloys—a review. *J. Mater. Res.* **33**, 3092–3128 (2018).
2. George, E. P., Raabe, D. & Ritchie, R. O. High-entropy alloys. *Nat. Rev. Mater.* **4**, 515–534 (2019).
3. Miracle, D. B. et al. Exploration and development of high entropy alloys for structural applications. *Entropy* **16**, 494–525 (2014).
4. Mott, N. F. & Nabarro, F. R. N. An attempt to estimate the degree of precipitation hardening, with a simple model. *Proc. Phys. Soc.* **52**, 86–89 (1940).
5. Labusch, R. Statistische Theorien der Mischkristallhärtung. *Acta Metall.* **20**, 917–927 (1972).
6. Senkov, O., Wilks, G., Scott, J. & Miracle, D. Mechanical properties of $Nb_{25}Mo_{25}Ta_{25}W_{25}$ and $V_{20}Nb_{20}Mo_{20}Ta_{20}W_{20}$ refractory high entropy alloys. *Intermetallics* **19**, 698 – 706 (2011).
7. Zou, Y., Maiti, S., Steurer, W. & Spolenak, R. Size-dependent plasticity in an $Nb_{25}Mo_{25}Ta_{25}W_{25}$ refractory high-entropy alloy. *Acta Materialia* **65**, 85 – 97 (2014).
8. Yao, H. et al. MoNbTaV medium-entropy alloy. *Entropy* **18**, 189 (2016).
9. Körmann, F. & Sluiter, M. H. Interplay between lattice distortions, vibrations and phase stability in NbMoTaW high entropy alloys. *Entropy* **18**, 403 (2016).
10. Yao, H. et al. Mechanical properties of refractory high-entropy alloys: experiments and modeling. *J. Alloy. Compd.* **696**, 1139 – 1150 (2017).
11. Dobbelstein, H., Thiele, M., Gurevich, E. L., George, E. P. & Ostendorf, A. Direct metal deposition of refractory high entropy alloy monbtaw. *Phys. Procedia* **83**, 624 – 633 (2016).
12. Kube, S. A. et al. Phase selection motifs in high entropy alloys revealed through combinatorial methods: Large atomic size difference favors bcc over fcc. *Acta Materialia* **166**, 677 – 686 (2019).
13. Ghoniem, N., Tong, M. S.-H. & Sun, L. Parametric dislocation dynamics: a thermodynamics-based approach to investigations of mesoscopic plastic deformation. *Phys. Rev. B* **61**, 913 (2000).
14. Zepeda-Ruiz, L. A., Stukowski, A., Oppelstrup, T. & Bulatov, V. V. Probing the limits of metal plasticity with molecular dynamics simulations. *Nature* **550**, 492–495 (2017).
15. Zepeda-Ruiz, L. A. et al. Atomistic insights into metal hardening. *Nat. Mater.* **20**, 315–320 (2021).
16. Daw, M. S. & Baskes, M. I. Embedded-atom method: derivation and application to impurities, surfaces, and other defects in metals. *Phys. Rev. B* **29**, 6443–6453 (1984).
17. Thompson, A., Swiler, L., Trott, C., Foiles, S. & Tucker, G. Spectral neighbor analysis method for automated generation of quantum-accurate interatomic potentials. *J. Comput. Phys.* **285**, 316–330 (2015).
18. Bertin, N., Zepeda-Ruiz, L. & Bulatov, V. Sweep-tracing algorithm: in silico slip crystallography and tension-compression asymmetry in bcc metals. *Mater. Theory* **6**, 1–23 (2022).
19. Stimac, J. C., Bertin, N., Mason, J. K. & Bulatov, V. V. Energy storage under high-rate compression of single crystal tantalum. *Acta Materialia* **239**, 118253 (2022).
20. Bertin, N., Carson, R., Bulatov, V. V., Lind, J. & Nelms, M. Crystal plasticity model of bcc metals from large-scale MD simulations. *Acta Materialia* **260**, 119336 (2023).
21. Chen, S. R. & Gray, G. T. Constitutive behavior of tantalum and tantalum-tungsten alloys. *Metall. Mater. Trans. A* **27**, 2994–3006 (1996).
22. Zhou, X. et al. Atomic scale structure of sputtered metal multilayers. *Acta Materialia* **49**, 4005–4015 (2001).
23. Vegard, L. Die Konstitution der Mischkristalle und die Raumfüllung der Atome. *Z. f.ür. Phys.* **5**, 17–26 (1921).
24. Varvenne, C., Luque, A., Nöhring, W. G. & Curtin, W. A. Average-atom interatomic potential for random alloys. *Phys. Rev. B* **93**, 104201 (2016).
25. Lin, D.-Y., Wang, S., Peng, D., Li, M. & Hui, X. An n-body potential for a Zr–Nb system based on the embedded-atom method. *J. Phys. Condens. Matter* **25**, 105404 (2013).
26. Li, X.-G., Chen, C., Zheng, H., Zuo, Y. & Ong, S. P. Complex strengthening mechanisms in the NbMoTaW multi-principal element alloy. *npj Comput. Mater.* **6**, 70 (2020).
27. Coury, F. G., Kaufman, M. & Clarke, A. J. Solid-solution strengthening in refractory high entropy alloys. *Acta Materialia* **175**, 66–81 (2019).
28. Maresca, F. & Curtin, W. A. Mechanistic origin of high strength in refractory bcc high entropy alloys up to 1900k. *Acta Materialia* **182**, 235–249 (2020).
29. Maresca, F. & Curtin, W. A. Theory of screw dislocation strengthening in random bcc alloys from dilute to high-entropy alloys. *Acta Materialia* **182**, 144–162 (2020).
30. Lee, C. et al. Strength can be controlled by edge dislocations in refractory high-entropy alloys. *Nat. Commun.* **12**, 1–8 (2021).
31. Rao, S., Woodward, C., Akdim, B., Senkov, O. & Miracle, D. Theory of solid solution strengthening of bcc chemically complex alloys. *Acta Materialia* **209**, 116758 (2021).
32. Louchet, F. & Kubin, L. Dislocation substructures in the anomalous slip plane of single crystal niobium strained at 50 k. *Acta Metall.* **23**, 17–21 (1975).
33. Christian, J. Some surprising features of the plastic deformation of body-centered cubic metals and alloys. *Metall. Trans. A* **14**, 1237–1256 (1983).
34. Stukowski, A. Visualization and analysis of atomistic simulation data with OVITO–the open visualization tool. *Model. Simul. Mater. Sci. Eng.* **18**, 015012 (2009).
35. Zhou, X., He, S. & Marian, J. Cross-kinks control screw dislocation strength in equiatomic bcc refractory alloys. *Acta Materialia* **211**, 116875 (2021).

36. Marian, J., Cai, W. & Bulatov, V. V. Dynamic transitions from smooth to rough to twinning in dislocation motion. *Nat. Mater.* **3**, 158–163 (2004).
37. Zhou, X., He, S. & Marian, J. Temperature dependence of the strength of Nb-Mo-Ta-W alloys due to screw dislocations. *Scr. Materialia* **239**, 115815 (2024).
38. Taylor, G. I. & Quinney, H. The latent energy remaining in a metal after cold working. *Proc. R. Soc. Lond. Ser. A* **143**, 307–326 (1934).
39. Saada, G. & Veyssière, P. in *Dislocations in Solids*. Vol. 11, 413–458 (Elsevier, 2002).
40. Kovács, I. The mechanism of the work-hardening in fcc metals. *Acta Metall.* **15**, 1731–1736 (1967).
41. Marin, M. Unloading effects in the plastic properties of copper single crystals. *Philos. Mag.* **3**, 287–301 (1958).
42. Marukawa, K. Dislocation motion in copper single crystals. *J. Phys. Soc. Jpn.* **22**, 499–510 (1967).
43. Cupp, C. R. & Chalmers, B. A study of the plastic deformation of copper single crystals. *Acta Metall.* **2**, 803–809 (1954).
44. Neurath, P. W. & Koehler, J. S. The plastic deformation of pure single crystals of lead and copper. *J. Appl. Phys.* **22**, 621–626 (1951).
45. Mitchell, T., Foxall, R. & Hirsch, P. Work-hardening in niobium single crystals. *Philos. Mag.* **8**, 1895–1920 (1963).
46. Mitchell, T. & Spitzig, W. Three-stage hardening in tantalum single crystals. *Acta Metall.* **13**, 1169–1179 (1965).
47. Madec, R. & Kubin, L. P. Dislocation strengthening in fcc metals and in bcc metals at high temperatures. *Acta Materialia* **126**, 166–173 (2017).
48. Kim, S., Svetlizky, I., Weitz, D. A. & Spaepen, F. Work hardening in colloidal crystals. *Nature* **630**, 648–653 (2024).
49. Thompson, A. P. et al. LAMMPS—a flexible simulation tool for particle-based materials modeling at the atomic, meso, and continuum scales. *Comp. Phys. Comm.* **271**, 108171 (2022).
50. Stukowski, A., Bulatov, V. V. & Arsenlis, A. Automated identification and indexing of dislocations in crystal interfaces. *Model. Simul. Mater. Sci. Eng.* **20**, 085007 (2012).
51. Pedregosa, F. et al. Scikit-learn: Machine learning in Python. *J. Mach. Learn. Res.* **12**, 2825–2830 (2011).
52. Labusch, R. A statistical theory of solid solution hardening. *Phys. Status Solidi (b)* **41**, 659–669 (1970).
53. Stukowski, A. Structure identification methods for atomistic simulations of crystalline materials. *Model. Simul. Mater. Sci. Eng.* **20**, 045021 (2012).

Acknowledgements

All authors thank C. Kalcher, A. Stukowski, L. A. Zepeda-Ruiz and S. Aubry for their generous help in data retrieval and analyses. The authors also acknowledge useful discussions with J. McKeown, T. Voisin, N. Bertin and A. Liang. X.Z., F.Z. and V.V.B. acknowledge funding support from the Laboratory Directed Research and Development program and a special computational time allocation on Lassen supercomputer from the Computational Grand Challenge program at Lawrence Livermore National Laboratory. This work was performed under the auspices of the U.S. Department of Energy by Lawrence Livermore National Laboratory under Contract DE-AC52-07NA27344.

Author contributions

V.V.B. developed the concept, F.Z. secured funding, X.Z. and V.V.B. ran MD simulations, X.Z. and F.Z. developed GPR models, all authors analyzed results and wrote the paper.

Competing interests

The authors declare no competing interests.

Additional information

Supplementary information The online version contains supplementary material available at https://doi.org/10.1038/s41524-026-01975-5.

Correspondence and requests for materials should be addressed to Xinran Zhou.